Design of Microfabricated Transformers and Inductors for High-Frequency Power Conversion

Charles R. Sullivan, *Student Member, IEEE,* and Seth R. Sanders, *Member, IEEE*

Abstract—**Transformers and inductors fabricated with micron-scale magnetic-alloy and copper thin films are designed for high-frequency power conversion applications. Fine patterning produced by photolithography reduces eddy current losses, thus enabling very high power densities. Calculated design graphs and design examples for 10-MHz transformers are presented.**

I. Introduction

ONE of the main difficulties in the miniaturization of power conversion circuits such as dc-to-dc converters is the construction of inductors and transformers. Increased switching frequency can, in general, lead to decreased requirements for the values of inductors and capacitors in power circuits. Transformer size can also be decreased at high frequency because of the reduced volt-seconds across each winding. However, as frequencies are pushed into the MHz region, several problems arise. Core materials commonly used in the 20–500 kHz region, such as MnZn ferrites, have rapidly increasing hysteresis and eddy current loss as the frequency is increased. Furthermore, eddy current losses in windings can also become a severe problem, as the skin depth in copper becomes small in relation to the cross section of wire used. Even if these problems are adequately dealt with, the resulting transformer and/or inductor is still one of the physically largest components and is likely to cost the most to manufacture.

In the magnetic recording industry, thin-film metal alloys are replacing ferrites as the material of choice for inductive read-write heads, particularly where high density and high frequency are required. These materials have high saturation flux density, and the use of thin films controls eddy current losses at high frequencies, up to frequencies above 100 MHz [1]–[3]. Structures with very small feature size are fabricated with integrated-circuit-like photolithography techniques [4]–[7]. The materials and the fabrication techniques used for magnetic recording heads show much promise for high-performance, high-frequency power conversion. The ability to accomplish very fine patterning can reduce eddy-current losses in both cores and windings. The higher-saturation flux density of the magnetic alloys, as compared with that of ferrites, allows high power density in small, planar devices. While costs may initially be high, batch processing techniques can bring the cost down to levels lower than with conventional wound magnetic circuit elements. In any case, the cost structure will be very different from that of conventional magnetic devices. The cost will be related to the number of layers and substrate area, rather than the volume of magnetic material and complexity and number of turns. This may mean that components needing a large number of turns will be more practical with microfabrication techniques.

Much previous work has been done on the design of planar high-frequency power transformers. Many of these transformers are made with relatively large-scale fabrication techniques and use ferrite cores. However, some recent research has produced several microfabricated transformers with thin-film magnetic metals. In [8], a power transformer is constructed using a thin (10 μm) metal film core. It achieves an efficiency of 78%, but at a low power density, $3\,\mathrm{mW/cm^2}$. In [9] and [10], a transformer fabricated with sputtered CoZrRe core material achieves a higher power density of about $0.72\,\mathrm{W/cm^2}$, and in [11] integrated Schottky rectifier diodes are added on the same substrate, demonstrating the feasibility of integrating magnetics and semiconductors. In [12] a design using a sputtered CoNbZr magnetic material achieves good efficiency and power density, with over 60% efficiency at 0.8 $\mathrm{W/cm^2}$ at 10 MHz.

In this paper, we discuss design and optimization procedures for high-frequency transformers using thin-film microfabricated transformers. Our results show that much higher power densities and efficiencies are possible in an optimized transformer, constructed using materials and processes similar to those used to construct magnetic recording heads. Design and optimization approaches for high-frequency transformers using these materials and processes are developed. Efficiency and power throughput are estimated for a range of designs and are worked out in detail for one example design.

Microfabricated magnetic components are expected to be useful for a wide range of applications. Our results are given in terms of power handling capability per unit substrate area for a specified efficiency level and can be used for any power level, simply by scaling the area. For high-power applications, a substrate might have the power semiconductors, capacitors, and control circuitry mounted on one side, and the microfabricated magnetics fabricated on the reverse side. Since the magnetics would be less than 100 μm-thick, a heat sink could be mounted on the same side of the substrate as the magnetics. Substrates with microfabricated magnetic devices could also be stacked to increase power handling. For low-power applications requiring a few watts, microfabrication would make it possible to use a transformer only a few

Manuscript received August 3, 1993; revised September 6, 1995. This work was supported in part by an NSF Graduate Fellowship, National Semiconductor, and the UC Micro program.

The authors are with the University of California, Berkeley, Department of Electrical Engineering and Computer Sciences, Berkeley CA 94720 USA.

Publisher Item Identifier S 0885-8993(96)01936-9.

millimeters square, allowing the entire converter to fit in a very small package.

It would also be desirable to be able to integrate magnetic components onto a silicon substrate along with other control and power circuitry. This would, for example, allow a power circuit to be added to a VLSI circuit, making the chip entirely self-sufficient, without requiring external support in the form of power supplies. Integration of a power circuit, even if it were for powering external circuitry or equipment, would offer advantages. For example, the short interconnections between the magnetic and other circuit elements would decrease the lead inductance which can otherwise cause problems at high frequencies.

Although we focus on power-handling magnetic components, there are potentially many other applications for microfabricated magnetic components. In power electronics, these applications could include small, high-Q inductors for resonant gate drive applications [13], [14]. The square hysteresis-loop characteristic of the magnetic materials is ideal for magnetic amplifier applications and other devices requiring these characteristics, such as some current sensors [15].

II. Magnetic Materials

Although ferrites are among the most popular materials for designing conventional high-frequency transformers, they are not easily integrated with microfabrication methods. The high-sintering temperatures of standard high-quality ferrites (1000–2000°C [16]) are difficult to combine with other steps of microfabrication techniques. However, other materials may actually be more desirable. The main advantage of ferrite over typical magnetic metal alloys is ferrite's high resistivity, which keeps eddy current losses to manageable levels at high frequency. The eddy current losses in magnetic alloys, however, can be controlled by using the alloys in thin-film form. Furthermore, ferrites can be run only at relatively low flux levels, both because they have low saturation flux densities and because rapidly increasing hysteresis losses limit ac flux to typically less than 0.1 T at frequencies over 1 MHz. Magnetic alloys used in recording heads have saturation flux densities over 1 T and usually can be operated close to this level without a loss penalty.

Probably the most common and best understood alloy for thin-film magnetics is permalloy, (82% Ni–18% Fe wt.%). It has a saturation flux density of 1.1 T at room temperature, and because of a relatively high Curie temperature (500°C), the saturation flux density degrades little at high temperature. It is down 10% at 130°C. Permalloy in bulk form has a resistivity of 20 $\mu\Omega$cm [17]. Films may be deposited by electroplating [18]–[20], sputtering [21]–[23], and other methods.

It is well known in the field of thin film magnetics that hysteresis loss in permalloy films can, in principle, be eliminated if changes in magnetization proceed by coherent rotation of the magnetization in a single domain, instead of by domain wall motion. This is achieved by controlling the magnetic anisotropy. We will briefly outline the principles of this, based on the discussion in [24] and [25]. Discussion of these effects is also contained in [26] and [27]. If a film is coherently magnetized, i.e., if all the domains are lined up in the same direction, the magnitude of the magnetization $\vec{M}$ will be the saturation magnetization, M_s. Since the magnetization has a strong tendency to stay in the plane of the film, $\vec{M}$ can be described by its angular direction in the plane of the film, θ

$$\vec{M} = M_s \cos\theta \hat{x} + M_s \sin\theta \hat{y}. \tag{1}$$

If the film is deposited or annealed in a magnetic field, parallel to one axis in the plane of the film, it develops a uniaxial anisotropy that can be described by the anisotropy energy

$$U_u = K_u \sin^2\theta \tag{2}$$

where θ is defined as the angle between the magnetization vector and the easy axis of magnetization determined by the applied field during annealing. The behavior of the film in an applied field can be understood by considering the total energy associated with a given angle of the magnetization vector, including the anisotropy energy and the energy associated with the applied field

$$U = K_u \sin^2\theta - H_x M_s \cos\theta - H_y M_s \sin\theta \tag{3}$$

where H_x and H_y are the components of the applied field in the easy and hard axis directions, respectively. At a stable equilibrium, $\partial U/\partial\theta = 0$, and $\partial^2 U/\partial\theta^2 > 0$. The first derivative condition results in

$$H_k \sin\theta\cos\theta + H_x \sin\theta - H_y \cos\theta = 0 \tag{4}$$

where H_k is a constant defined as $H_k = 2K_u/M_s$. In general one might expect to find that multiple stable solutions would lead to a multiple-valued B-H curve. For an applied field in the hard axis direction, however, (4) reduces to $H_y/H_k = \sin\theta$, and so $M_y = \sin\theta M_s = M_s H_y/H_k$. This holds for $|H_y| < H_k$ and results in the lossless hysteresis loop shown in Fig. 1. Although there are multiple solutions for θ, they result in the same value for M_y. For an applied field in the easy axis direction, on the other hand, multiple solutions result in the multiple-valued, and so lossy, hysteresis loop shown in Fig. 2. For our applications the hard axis loop is preferred. In practice it may be best to orient the hard axis a few degrees away from the expected direction of the applied field, to help maintain a single magnetic domain. Although the hysteresis loops shown in Figs. 1 and 2 were measured at low frequency, behavior at frequencies up to 100 MHz is very similar. Thus, coherent rotation can be used to almost completely eliminate hysteresis loss.

Another alloy commonly used for recording heads is sendust (FeAlSi). Its principal advantage for recording heads is its higher wear resistance, but it also has higher resistivity than NiFe, 90–119 $\mu\Omega$cm [28], [29]. Numerous other materials are under development for higher performance magnetic recording heads. Although many of the requirements for magnetic recording heads are similar to those for power applications, in several respects, the requirements for power applications are less severe. In particular, mechanical wear resistance, corrosion resistance and thermal stability are all very important for magnetic recording heads. In power applications, however,

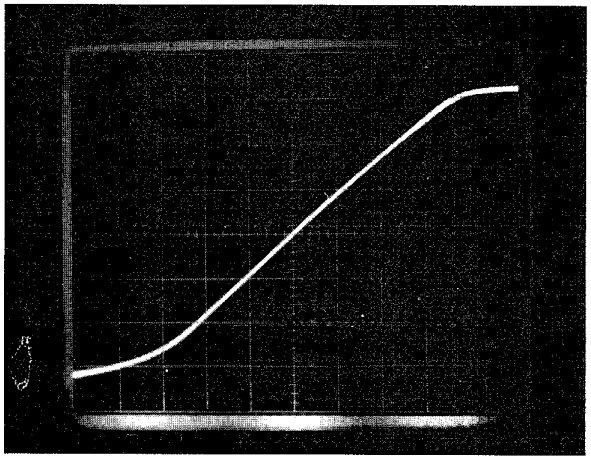

Fig. 1. Experimental NiFe hard axis hysteresis loop, X: H, .85 Oe/div, Y: B, uncalibrated.

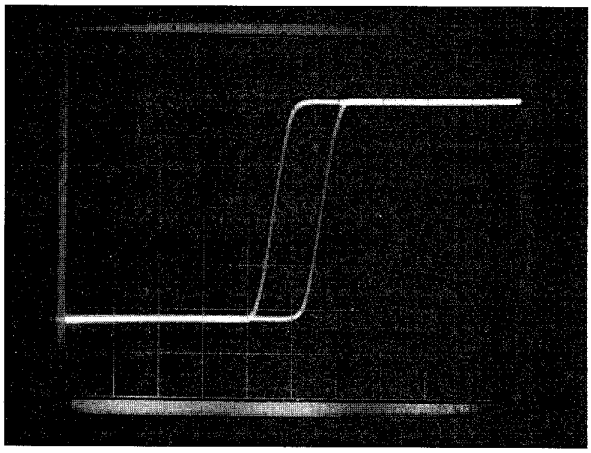

Fig. 2. Experimental NiFe easy axis hysteresis loop. X: H, .85 Oe/div, Y: B, uncalibrated.

the component is not subject to mechanical wear, and it can be sealed from the atmosphere to resist corrosion. Thermal stability is particularly important in Metal-In-Gap (MIG) recording heads, in which the high-saturation flux density material is bonded at high temperatures to the main body of the core. Such a high-temperature process would not be used in manufacturing power components. Thus some of the materials that are impractical for use in heads may be excellent for power applications. For example, FeN compounds have shown saturation flux densities above 2.8 T, and very low coercivity, under 0.3 Oe. The major drawbacks for recording head applications are their low corrosion resistance and low thermal stability. The addition of aluminum to these materials improves their thermal stability, while maintaining a high-saturation flux density of 2 T [30]. Many other materials being developed for recording head applications also show excellent coercivity and saturation flux density and may be excellent for power applications [1], [2].

In order to increase flux-carrying capacity without detrimental increases in eddy current loss, one may use layers of magnetic alloy, separated by a dielectric such as SiO_2 or AlO_2,

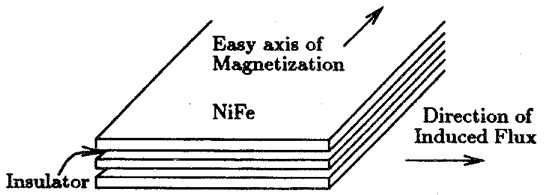

Fig. 3. Laminated core structure.

as shown in Fig. 3. In some recording-head materials, this also results in decreased coercivity [1], [2], [30].

III. Geometry

Any transformer, made by a process of alternately depositing conductor or magnetic material, must have at least two steps of conductor deposition or two steps of core deposition in order to interlink the core and coil. Designs in either category may be considered variations or combinations of the basic constructions in Figs. 4 and 5, which we call pot-core and toroidal designs, respectively, because of their general resemblance to conventional pot-core and toroidal transformers.

In order to rigorously compare the power handling capability of the two designs, one must perform complete design optimization calculations, as discussed in the following sections. The result shows that the pot-core design can handle more power in the same area. In order to make this result more intuitive, we also consider a simpler situation. We compare a pot-core and a toroidal design, each with the same layer thicknesses: each conductor layer in the toroidal design the same thickness as the one conductor layer in the pot-core design, and each core layer in the pot-core design the same thickness as the one core layer in the toroidal design. As shown in Appendix I, at low power density, the two designs have the same efficiency, with the ratio of flux density and current density in each set to maximize efficiency. However, with the same power density, the toroid has a higher flux density. It will be shown that optimal designs will always be limited by saturation. This can explain the higher power handling capability of the pot-core design.

Sometimes an important issue in choosing a core shape is the magnitude and distribution of external magnetic fields generated by the transformer. The pot core is often the best design for this because the core encloses and so shields the windings. The result is low external fields regardless of the distribution of primary and secondary windings inside the core. Toroidal transformers also often have low external fields. This is more a result of the winding distribution than of the core shape, however. The primary and secondary winding are customarily both distributed evenly around the core, lying on top of each other with little space between. Thus the currents, as seen from even a short distance away, very nearly cancel each other, and so little external field results. Second, the effects of magnetizing current producing external fields are minimized because the MMF produced by the winding is dropped locally in the same portion of the core, and thus no two regions of the core are at MMF's that differ by more than the current in one turn.

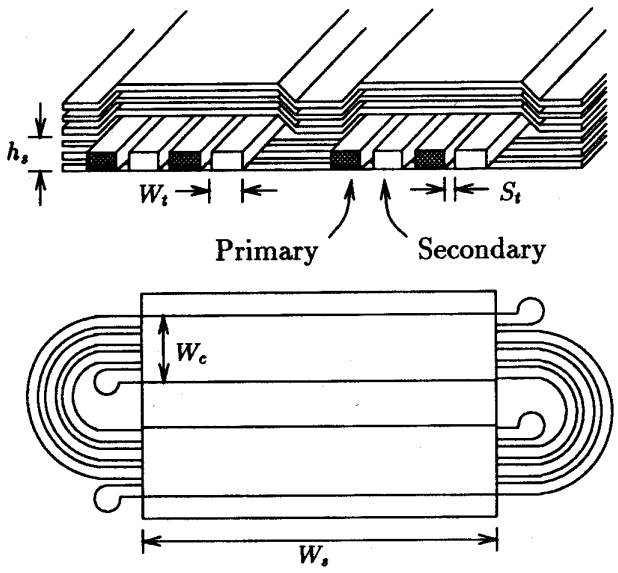

Fig. 4. Pot-core structure.

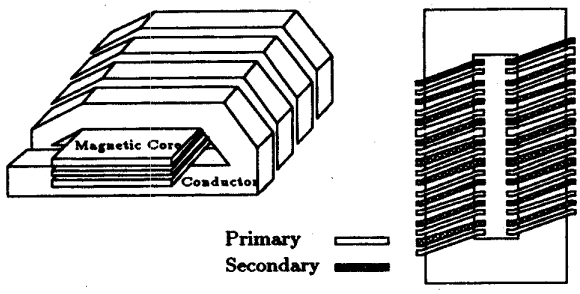

Fig. 5. Toroidal structure.

In microfabricated transformers, the ability to finely pattern windings makes it relatively easy to arrange the windings so that primary and secondary currents locally cancel. Thus the first advantage of toroidal-core transformers is easily realized, even in nontoroidal shapes. With a high-permeability core material such as NiFe, magnetizing current can be relatively small, making the second advantage of toroids unimportant. Thus external fields are not a primary concern in choosing geometry.

Perhaps the most important parameter to consider in comparing pot-core and toroidal designs is ease of fabrication. This is also the most difficult to quantify, but it appears that pot-core design is overall easier to fabricate, as discussed below. It is also more similar to recording head designs and so is better proven.

In the toroidal-core design, a difficulty is connecting the bottom and top layers of conductor to encircle the core. This requires that the registration between the layers is adequate to insure proper connections, requires low-resistance contacts and requires connection over a vertical distance equal to the thickness of the core. None of these are beyond the capabilities of present technology, but all add some difficulty or complexity. In [31] low-resistance contacts over a large vertical distance around the core are achieved by electroplated vias with carefully cleaned contact surfaces.

In the pot-core design, the interlayer connection requirements are in one sense less severe, because connections to particular individual wires are not required, and small gaps of insulator would not be a problem as the area can be made sufficiently large that the gap reluctance is negligible. However, if the thickness of the conductor layers is larger than the thickness of the core layers (which will be the case in our designs) the vertical distance over which connections must be made is larger in the pot-core design. There is also an additional connection that must be made. Unless the transformer has only one turn, the winding will be a spiral, and there must be a connection to the center of the spiral. This would typically involve a fourth deposition step, or the use of external connections such as bond wires. Series and parallel combinations of single-turn structures are a possible way to avoid this difficulty.

In an NiFe toroidal core, the orientation of the easy axis of magnetization may be difficult. In a circular core, the desired easy axis direction is radial in a circular core. Fabrication of a such a device is difficult, but may be possible [32]. In a square core, there are only two different directions needed, but it would still be very difficult to achieve the precise localized fields needed to fabricate this. A long rectangular core could be used, with the easy axis oriented a few degrees from perpendicular to the length of the core. For most of the core, it would be properly oriented. However, for the ends of the core, it would be oriented in the unfavorable direction, resulting in high losses due to the easy-axis hysteresis loop. It should then be made as long and thin as is practical to minimize these end losses.

In the pot-core design, the easy axis orientation is not difficult if, again, the shape is long and rectangular, with the turns going around the end uncovered by any core material, as shown in Fig. 4. A problem, however, is that the flux must cross perpendicular to the sheets to get from the top layers of NiFe to the bottom layers. Flux in this perpendicular direction will produce some eddy current losses.

Overall, the pot-core design appears to be superior because it can handle higher power, has fewer difficulties with interconnecting different layers of conductor, and can easily have the magnetic anisotropy oriented correctly.

IV. Winding Design

In this section, design of transformer windings for the lowest possible loss is discussed, considering high-frequency skin effect and proximity effect losses, and the limitations imposed by microfabrication techniques. Throughout this discussion it will be assumed that the actual number of turns is of little consequence. As long as the overall structure is large enough that there are many turns, the effective number of turns can be adjusted at will by putting turns in series or parallel, by making minor adjustments to the overall size, and even by putting entire microtransformers in series or parallel. The parameter to be minimized is not simply R, but rather R/n^2, where n is the number of turns and R is the overall winding resistance.

We assume it is necessary to fabricate the windings in a single layer for the pot-core design, in order to minimize the cost. In this case, an important constraint in the winding design is the spacing between windings. This may be constrained by the vertical to horizontal aspect ratio achievable with the photolithography process used. For example, with a plated height of 20 μm, and a 1 : 4 aspect ratio, the minimum spacing between conductor segments is 5 μm. In some cases the minimum spacing may be set by other constraints, for example where very high voltage isolation or low capacitance between primary and secondary is needed. For example, SiO_2 has a dielectric strength between 300 and 1000 V/μm [33], [34]. A 5-μm thickness may be adequate for some applications, but depending on the derating factor used and the voltage requirements, greater thickness may be needed.

Simple dc R/n^2 minimization would dictate that the conductor should be as wide as possible, and the space between conductors as narrow as possible consistent with the constraint (e.g., 5 μm). However, for high-frequency currents, skin effect becomes important, and when the conductor gets wide compared to the skin depth, it is not effectively utilized. Thus there is an optimal width, between very small widths where too much of the cross-sectional area is wasted by the interwinding space, and large widths where skin effect and proximity effect increase the losses. For both the pot-core and toroidal geometries under consideration, the skin effect and proximity effect losses can be described by an ac resistance, determined by multiplying the dc resistance by a factor F_r, which can be approximated by

$$F_r = 1 + \frac{5p^2 - 1}{45}\psi^4 \tag{5}$$

where p is the number of layers, and ψ is the ratio of conductor thickness-to-skin depth [16], [35]. Interleaving primary and secondary windings is desirable for a low value of p. Simple interleaving as shown in Fig. 4 results in $p = 1$. To minimize ac resistance, we adjust the width of the individual conductor turns, W_t, to minimize a resistance factor, F'_R, that takes into account both the reduction in conductor area due to spacing between windings

$$F'_r = F_r \frac{W_t + S_t}{W_t} \tag{6}$$

where S_t is the spacing between turns, determined by the aspect ratio. At 10 MHz, for example, copper has a skin depth of 22 μm, and F'_r takes on a minimum value of 1.32 with $W_t = 19.8$ μm and $F_r = 1.054$, for $S_t = 5$ μm.

If more than one layer can be used for the winding, the primary and secondary may be wide ribbons, on top of one another. In this case the above optimization is unnecessary, but the fabrication requires more steps.

V. Laminations

Similar to losses in the conductor, eddy current losses in the core are decreased by making finer laminations, but making them fine also sacrifices cross-sectional area and so increases the flux density, which increases losses and can lead to saturation. An appropriate compromise must be found.

Eddy current power loss may be easily estimated if it is assumed that the field distribution is not affected by the induced current, and so is uniform throughout the cross section of the lamination. This is ordinarily a good assumption if the thickness of the lamination is small compared with a skin depth. At 10 MHz, the skin depth in NiFe with a permeability of 2000 is about 3 μm. Furthermore, in thin films on the order of 1 μm, the uniformity of the field is enhanced by spin coupling [25]. Thus the expression

$$P_{\text{loss}} = \frac{\omega^2 B^2_{\text{peak}} V d^2}{24\rho} \tag{7}$$

where V is the volume and d is the lamination thickness, is a good approximation.

Since the cost of fabrication is likely to be very dependent on the number of layers, we take the number of layers as given and optimize the thickness of the layers. Given this, the cross-sectional area and volume of core material are proportional to the thickness of the laminations. For a given total flux, B is inversely proportional to the thickness. Since B and the thickness of the laminations both appear squared in the loss, those terms cancel, and the only overall effect of thickness on total loss is through the volume term. Thus, the thickness should be chosen as small as possible, consistent with avoiding saturation.

VI. Transformer Design

There are many possible design methodologies. For instance, one may choose a power throughput density objective, and find the maximum efficiency design meeting that objective. Or one may start with an efficiency objective and find the maximum power throughput density possible at that efficiency. We will choose the latter, in part because it is easier to come up with an efficiency objective *a priori*.

With a winding height, winding spacing and width, and number of core layers fixed, the only important remaining choices for a rectangular geometry are the height of the core (h_s, s for steel), the voltage, the current, the width of the core (W_s), and the width of the windings, (W_c, c for conductor). In practice, there would be fixed requirements for current and voltage, and the overall size and number of turns would be adjusted to match these. However, for the purposes of determining the throughput possible at a given efficiency, we will assume that the number of turns is fixed and adjust both the voltage and current. If the width of the windings and core are large enough, the throughput per substrate area becomes a very weak function of those widths. We assume, for approximate calculations, that the edge and end losses are negligible, and so the efficiency and throughput are independent of W_c and W_s. This assumption is verified on an example design, below.

Any optimal design will have the flux density at the saturation flux density of the core, although in practice, some safety margin will be allowed. This is because if the flux density were below the maximum allowed, the voltage and current could be scaled up together, increasing the power handling without affecting the efficiency. Thus, for any given core

height, the optimal voltage per turn is easily calculated. Given an efficiency requirement, the optimal core height (which determines an optimal voltage), and the maximum current for that efficiency, may be calculated. In Appendix II this is shown to result in a power density

$$P/A = \frac{7962624}{3125\pi^{12}} \frac{(1-\eta)^5 N^4 h_c^3 w^2 B_{pk}^2 \rho_s^2}{\rho_c^3 F_R'^3} \tag{8}$$

with all quantities in SI units, for a transformer with square voltage waveforms and sinusoidal current waveforms. This expression is valid for laminations thin enough that the approximation of uniform B used to calculate eddy current loss is valid. It also assumes negligible hysteresis losses and sufficiently high permeability that magnetizing current is negligible. Note that the power density is very sensitive to the conductor losses, as indicated by the appearance of the cubes of conductor resistivity, height, and F_R'. It is even more sensitive to the number of layers, N, and to the efficiency, η.

VII. Example Design

In this section, the design methods discussed in the last section are applied to pot-core transformer designs based on a permalloy or sendust core materials with copper conductors. We consider transformer designs for a series resonant converter, operating at 10 MHz. The assumption of a series resonant converter is needed only to determine the current and voltage waveforms in the transformer. Performance with other types of converters would be similar.

The core height was limited to a maximum total height of each half of 20 μm, with a maximum lamination thickness of 3 μm. Copper plating height was limited to 20 μm. A maximum flux density of 1 T was used. Although resistivity of thin films of plated copper is often higher than copper's bulk resistivity, a thickness of 20 μm is sufficient to achieve a resistivity very close to the copper's bulk resistivity of 1.7 $\mu\Omega$-cm [36]–[38]. We conservatively base our designs on a resistivity of 2.0 $\mu\Omega$-cm. Since the NiFe core material is in much thinner layers, a maximum of 3 μm thick, it may show a significant increase in resistivity. Nonetheless, we conservatively base our calculations on its bulk resistivity of 20 $\mu\Omega$ cm.

Based on these assumptions, the calculations outlined in Appendix II were used to find power density as a function of efficiency. The results are shown in Figs. 6–8 for transformers with one, four, or 10 layers of NiFe laminations. The number of layers has a strong influence on the performance. With one layer, power density ranges from under 10 $\mathrm{mW/cm^2}$ at 95% efficiency to 6 $\mathrm{W/cm^2}$ at 80% efficiency. With 10 layers, 60 $\mathrm{W/cm^2}$ is achievable at 95% efficiency, and over 1000 $\mathrm{W/cm^2}$ is possible at 80% efficiency.

Fig. 9 is based on the same type calculation and shows the possibilities offered by a higher-resistivity magnetic material, such as sendust. Sendust's resistivity was taken as 105 $\mu\Omega$-cm, and it was used at a maximum flux density of 1 T. The calculated performance of a four-layer transformer was almost as good as a 10-layer permalloy transformer.

To make the information shown in Figs. 6–9 more concrete, a design for a typical transformer has been performed and

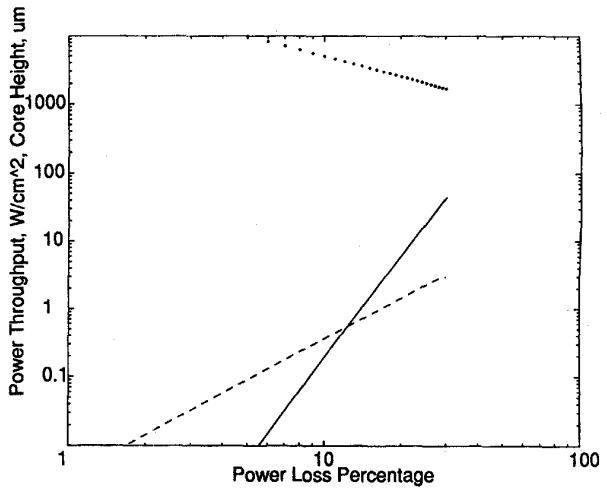

Fig. 6. Theoretical power throughput as a function of efficiency with a one-layer NiFe core in a pot-core design (solid line). Core height, h_s, for maximum power throughput is shown as a dashed line. The descending dotted line shows a thermal dissipation limit of 500 $\mathrm{W/cm^2}$.

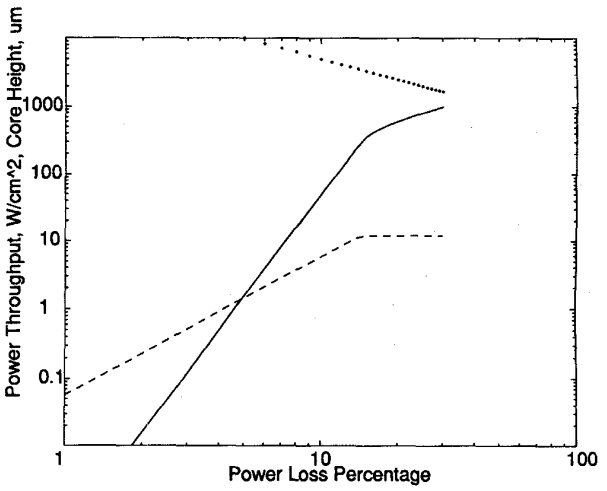

Fig. 7. Theoretical power throughput as a function of efficiency with a four-layer NiFe core in a pot-core design (solid line). Core height, and a thermal dissipation limit are also shown, as in Fig. 6.

analyzed. Fig. 8 shows that a device with 10-layer laminations can achieve a power throughput of 60 $\mathrm{W/cm^2}$ at a theoretical efficiency of 95%. This is achieved with a lamination layer height of 0.9 μm, for a total height of NiFe of about 9 μm. Dimensions are chosen for an approximate total substrate area of 6 mm $\times$ 1 mm and are adjusted to fit an integral number of optimal-width turns. Using the final dimensions shown in Table I, the actual efficiency and power density were calculated and are shown in Table II. The actual efficiency includes hysteresis losses and the losses in the end turns of conductor and in the overhang of the core. Hysteresis losses are assumed to be due to a parallelogram hysteresis loop with coercivity of 0.03 Oe. The magnetizing current was also calculated, but because of the high permeability of the NiFe, it contributes only slightly to the conductor loss. The substrate area is the

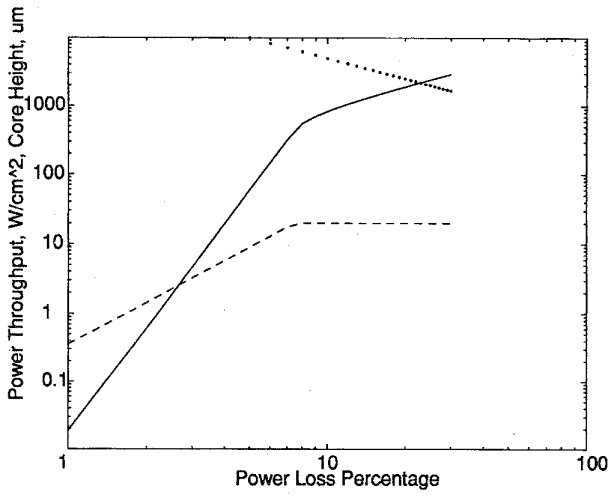

Fig. 8. Theoretical power throughput as a function of efficiency with a 10-layer NiFe core in a pot-core design (solid line). Core height and a thermal dissipation limit are also shown, as in Fig. 6.

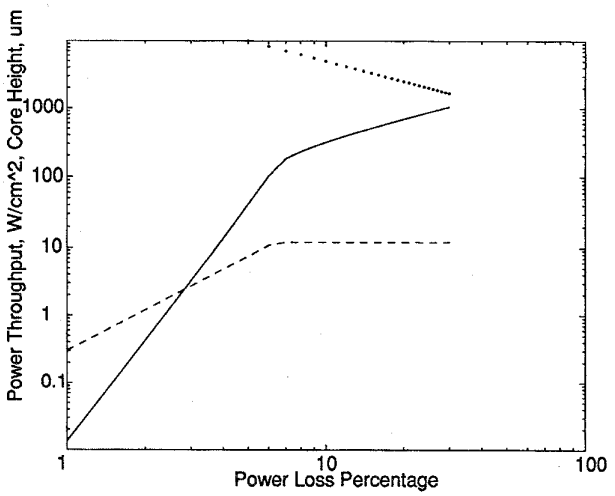

Fig. 9. Theoretical power throughput as a function of efficiency with a four-layer sendust laminated core (solid line). Core height and a thermal dissipation limit are also shown, as in Fig. 6.

area of a rectangle enclosing the entire structure, including the end turns and core overhang.

VIII. Power Dissipation

Often an important parameter in power transformer design is the allowable temperature rise, determined by power dissipation and thermal resistance, typically from the transformer to the surrounding air. Small transformers (on the order of 10 cm^3) are typically limited more by efficiency requirements than by temperature rise. This is also true of the microfabricated transformers discussed here. Typical power semiconductors are rated to dissipate about 500 W/cm. With similar mounting and heatsinking techniques, similar power dissipation should be possible for microfabricated transformers. Dissipation of 500 W/cm^2 is far above the typical dissipation of our designs of around 10 W/cm^2. Figs. 6–8 show a 500 W/cm^2 limit as a dotted line. Only very low-efficiency, high-power-density, many-layered designs exceed this limit.

TABLE I
Parameters of Example Design

Symbol		Value
W_c	Width of conductor	490 μm
W_t	Width single turn	19.8 μm
S_t	Spacing of turns	5 μm
W_s	Width of core	5.02 mm
h_c	Height of conductor	20 μm
h_s	Height of core	8.96 μm
h_s/N	Thickness of core layer	.896 μm
h_d	Thickness of dielectric between conductor and core	5 μm
N	Number of layers of core	10
n	Number of turns in primary = number of turns in secondary	10
A	Substate area	0.064 cm^2
f	Operating frequency	10 MHz
B	Peak flux density	1.0 T
ρ_c	Conductor (Cu) resistivity	2.0 $\mu\Omega - cm$
ρ_s	Core (80% NiFe) resistivity	20 $\mu\Omega - cm$
μ	Core permeability	2000 μ_0

IX. Inductors

Inductors are also essential in switching power converters. Perhaps the simplest way to build a microfabricated inductor would be to use the pot-core geometry and introduce a gap between the top and bottom sections of core. Unfortunately, this sandwich design leads to very high eddy current losses in the conductor, because of the distribution of the field in the region of the windings [39], [40], [41]. For ac inductors, this has led to the use of meander coils [42], [43], [44], which are effectively many single-turn structures in series. Since a single-turn inductor does not have proximity effect problems, this is effective in decreasing losses. However, in order to effectively utilize the magnetic material and in order to get a high inductance, the gap reluctance in the magnetic path around each conductor must be reasonably small [42]. In microfabricated designs, this would require spacing the conductors widely enough to allow the top layer of magnetic

TABLE II
CALCULATED ELECTRICAL PERFORMANCE OF EXAMPLE DESIGN

Symbol		Value
P	Power throughput	2.98 W
	Theoretical power density	59.3 W/cm^2
	power density decrease from:	
$\Delta(P/A)$	End-turn area	-9.4W/cm^2
$\Delta(P/A)$	Core overhang area	-3.3 W/cm^2
P/A	Net power density	46.6 W/cm^2
	Eddy current loss in core	60.7mW
	Hysteresis loss in core	8.8 mW
R	DC resistance (of either winding)	5.85 Ω
R_{ac}	AC resistance	6.17 Ω
L_m	Magnetizing Inductance	22.2 μH
i_m	Magnetizing Current	23.3 mA rms
i_p	Current (in primary)	95 mA rms
i_s	Current (in secondary)	92 mA rms
	Total conductor losses	108 mW
v	Voltage	36.0 V
P_{loss}	Total power loss	177 mW
	Theoretical Efficiency	95 %
$\Delta\eta$	End turns	-0.5 %
$\Delta\eta$	Core loss in overhang area	-0.04 %
$\Delta\eta$	Magnetizing current	-0.11 %
$\Delta\eta$	Hysteresis loss	-0.25 %
η	Net efficiency	94.1%

metal to come down close to the bottom layer. This decreases the area available for conductor and so increases the area needed for the complete device. Nonetheless, it is a viable option. An alternative fabrication approach for meander coils involves patterning the core in the same pattern as the coil. In this way, the need for insulation between the core and coil is eliminated [45], [46].

Proximity effect losses in a multiturn planar pot-core inductor can be almost completely eliminated by using a low-permeability material across the top of the windings to serve the function of a gap and maintain a favorable field configuration for low losses in the windings [41]. One way of making relatively low permeability core materials is to finely powder a magnetic alloy and then press the powder into a core. This

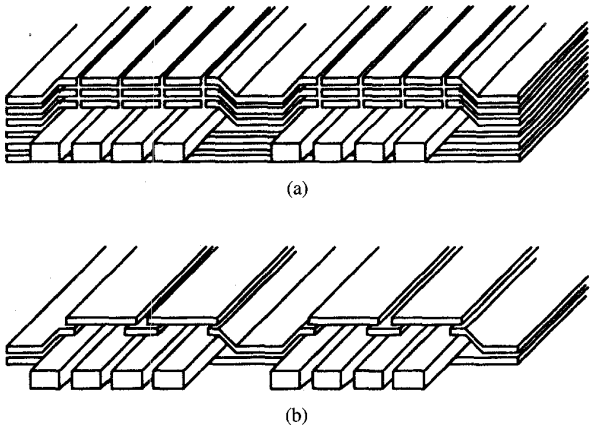

Fig. 10. Microfabricated inductors with quasi-distributed gap.

puts in many small air gaps. A problem with this is that the grains of magnetic material are randomly shaped and spaced, and as a result, some portions have higher flux densities than others. This makes linearity and low loss hard to achieve. With microfabrication techniques, the gaps could be put in much more precisely, achieving better characteristics. An equivalent of lower permeability material can be made by simply putting small gaps at regularly spaced intervals, forming a quasi-distributed gap. Fig. 10 shows examples of two such designs for a microfabricated inductor. This is similar in concept to the quasi-distributed gap used in [47], but microfabrication makes the use of multiple gaps easier, and the planar structure makes them more important. Fabricating the gaps by overlapping layers of magnetic material, as shown in Fig. 10(b) may make precise control of very small gap lengths easier. A two-dimensional finite-element magnetic field analysis was used to evaluate the losses in a structure like Fig. 10(a), operated at 10 MHz. Spacing between conductors and between the conductors and the core was 5 μm, the gaps were each 1μm, and each conductor was 35 μm wide by 20 μm high. The core was assumed to be ideal, lossless material 8 μm thick. The conductor losses were only 8% higher than the dc losses with the same current, corresponding to a value of F_R of 1.08. This shows that the design does in fact control eddy current losses very effectively. For comparison, a similar geometry, but with the gap at one edge only, had losses over four times as high.

X. CONCLUSION

Microfabricated magnetic components with NiFe or other metal-alloy cores show much potential as components in high-frequency power converters. The high-saturation flux density of these materials, combined with the ability to reduce eddy current losses by making microscopic laminations, allows very high power densities to be achieved. A pot-core-like structure with multiple horizontal layers of alloy, separated by insulator, appears to be the most desirable configuration. A design methodology is developed for choosing optimal conductor widths and core height. The approximate range of power density with a 10-layer core includes over 1000 W/cm^2 at 80% efficiency, and 95% efficiency at 60 W/cm^2. An example

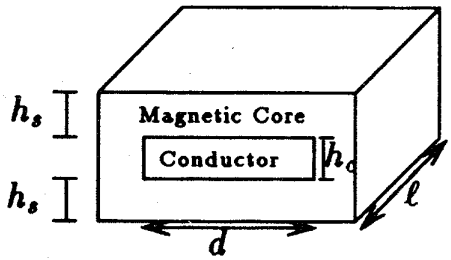

Fig. 11. Basic geometry considered.

design is worked out in detail, and achieves 94% efficiency at 46 W/cm^2 with a 10-layer core.

Appendix I
Comparison of Loss in Pot-Core and Toroid-Core Structures

First consider a section of copper surrounded by core, as shown in Fig 11. We assume that the conductor path is closed but ignore any deviations from the above geometry where the core turns corners. We also ignore any core loss in the sections at the left and right edges. We calculate the resistance and flux density

$$R = \frac{\ell \rho_c}{d h_c} \tag{9}$$

$$B = vt/\ell h_s \tag{10}$$

where t is the time of one quarter period of a square voltage waveform of amplitude v

$$P_{\text{core loss}} = 2K_{\text{core}} B^2 \ell h_s d \tag{11}$$

where K_{core} is a loss constant for the core material.

$$P_{\text{total loss}} = \frac{2K_{\text{core}} dt^2 v^2}{\ell h_s} + i_{\text{rms}}^2 R. \tag{12}$$

For a given transformer VA product, P, the total loss is minimized at

$$v = \left(\frac{\ell^2 \rho_c P^2 h_s}{d^2 h_c t^2 2K_{\text{core}}} \right)^{1/4} \tag{13}$$

which results in loss

$$P_{\text{total loss}} = 2\sqrt{2} t P \sqrt{\frac{K_{\text{core}} \rho_c}{h_s h_c}} \tag{14}$$

and flux density

$$B = \left(\frac{\rho_c P^2 t^2}{2d^2 h_c h_s^3 K_{\text{core}} \ell^2} \right)^{1/4}. \tag{15}$$

Now consider a section of core surrounded by copper with the identical geometry, except with h_c and h_s swapped so that h_c is still the conductor height and h_s is still the core height.

$$R = \frac{2d\rho_c}{\ell h_c} \tag{16}$$

$$P_{\text{total loss}} = \frac{K_{\text{core}} \ell t^2 v^2}{d h_s} + i_{\text{rms}}^2 R. \tag{17}$$

For a given transformer VA product, P, the total loss is minimized at

$$v = \left(\frac{2d^2 \rho_c P^2 h_s}{\ell^2 h_c t^2 K_{\text{core}}} \right)^{1/4} \tag{18}$$

which results in exactly the same loss

$$P_{\text{total loss}} = 2\sqrt{2} t P \sqrt{\frac{K_{\text{core}} \rho_c}{h_s h_c}} \tag{19}$$

but results in a higher flux density, by a factor of the square root of two

$$B = \left(\frac{2\rho_c P^2 t^2}{d^2 h_c h_s^3 K_{\text{core}} \ell^2} \right)^{1/4}. \tag{20}$$

Note that interchanging h_s and h_c makes no difference in the loss but does affect the flux density.

Appendix II
Calculation of Optimum Core Height and Maximum Power Troughput for a Given Efficiency

We perform this calculation for a horizontal-sheet-lamination pot-core design, such as in Fig. 4. Given an efficiency, η, and assuming a core height, h_s, we calculate the maximum current density, σ, which gives that efficiency or better, based on a similar geometry to that shown in Appendix I, ignoring all end and edge effects

$$W_s h_s B_{pk} = \int v(t)\, dt \tag{21}$$

where B_{pk} is the peak flux density, and W_s is the width of the magnetic material, as shown in Fig. 4. For a square-wave voltage, of amplitude v

$$\int v(t)\, dt = \frac{v\pi}{2\omega}. \tag{22}$$

The power throughput per area is

$$P/A = k_p \frac{v i_{\text{rms}}}{W_s W_c} = k_p \frac{2}{\pi} \omega h_s B_{pk} \sigma_{\text{rms}} \tag{23}$$

where k_p is the power factor, where W_c is the width of conductor, as shown in Fig. 4, i_{rms} is the rms current in one winding, and σ_{rms} is defined as i_{rms}/W_c. If the number of layers of laminations is N (per section, $2N$ overall for a pot core), the thickness of each layer is h_s/N

$$P_{\text{loss}}/A = \frac{2h_s \omega^2 B_{pk}^2 (h_s/N)^2}{24\rho_s} + 4F_R' \sigma_{\text{rms}}^2 \rho_c / h_c. \tag{24}$$

The factor of two in the first term is due to the two sections of core in a pot core. F_R' is a resistance factor taking into account both the ac resistance factor F_R, and the loss of winding space due to gaps between turns. The factor of four in the second term is due to the fact that there are two windings, each with twice the resistance that a single winding occupying the same space would have. Setting $(1-\eta)$ equal to the loss divided by the power throughput gives

$$(1-\eta) k_p \frac{2}{\pi} \omega h_s B_{pk} \sigma_{\text{rms}} = \frac{2h_s^3 \omega^2 B_{pk}^2}{N^2 24 \rho_s} + \frac{4F_R' \rho_c}{h_c} \sigma_{\text{rms}}^2. \tag{25}$$

Solving this quadratic equation for $\sigma_{\rm rms}$ gives

$$\sigma_{\rm rms} = \frac{h_c h_s (1-\eta) k_p B_{pk} \omega}{4\pi \rho_c F'_R} \cdot \left[1 + \sqrt{1 - \frac{\pi^2 F'_R \rho_c h_s}{3(1-\eta)^2 k_p^2 N^2 \rho_s h_c}}\right] \quad (26)$$

where we have chosen the large valued root, because we want to choose the largest current, and so power density, at which the chosen efficiency is achieved. The power per area is then calculated by substituting $\sigma_{\rm rms}$ into (23) to get

$$P/A = \frac{k_p^2 (1-\eta) h_c \omega^2 B_{pk}^2}{2\pi^2 \rho_c F'_R} h_s^2 \cdot \left[1 + \sqrt{1 - \frac{\pi^2 F'_R \rho_c h_s}{3(1-\eta)^2 k_p^2 N^2 \rho_s h_c}}\right]. \quad (27)$$

To find the optimal value of h_s, we set the derivative of this expression with respect to h_s equal to zero, obtaining

$$h_{s\rm opt} = \frac{72(1-\eta)^2 \rho_s k_p^2 N^2 h_c}{25\pi^2 \rho_c F'_R}. \quad (28)$$

Substituting this into (27) results in an expression for the power density with the optimal value of h_s

$$P/A = \frac{15552}{3125\pi^6} \frac{k_p^6 (1-\eta)^5 N^4 h_c^3 w^2 B_{pk}^2 \rho_s^2}{\rho_c^3 F'^3_R}. \quad (29)$$

For our examples, we assumed a sinusoidal current, in combination with the square-wave voltage assumed above. This results in a power factor $k_p = 2\sqrt{2}/\pi$, and (29) becomes

$$P/A = \frac{7962624}{3125\pi^{12}} \frac{(1-\eta)^5 N^4 h_c^3 w^2 B_{pk}^2 \rho_s^2}{\rho_c^3 F'^3_R}. \quad (30)$$

For generating Figs. 6–9, the maximum h_s was constrained to 20 μm, and the maximum thickness per lamination was constrained to 3 μm. If those constraints were violated, h_s was set to the maximum, and (27) used to calculate the power density.

REFERENCES

[1] T. Jagielinski, "Materials for future high performance magnetic recording heads," *MRS Bull.*, vol. 15, no. 3, pp. 36–44, Mar. 1990.

[2] O. Kohmoto, "Recent developments of thin film materials for magnetic heads," *IEEE Trans. Magn.*, vol. 27, no. 4, pp. 3640–3647, July 1991.

[3] K. P. Ash, D. Wachenschwanz, C. Brucker, J. Olson, M. Trcka, and T. Jagielinski, "A magnetic head for 150 MHz, high density recording," *IEEE Trans. Magn.*, vol. 26, no. 6, pp. 2960–296, Nov. 1990.

[4] E. P. Valstyn and L. F. Shew, "Performance of single-turn film heads," *IEEE Trans. Magn.*, vol. MAG-9, no. 3, pp. 317–326, Sept. 1973.

[5] J.-P. Lazzari, "Integrated magnetic recording heads applications," *IEEE Trans. Magn.*, vol. 9, no. 3, pp. 322–326, Sept. 1973.

[6] H. Schewe and D. Stephani, "Thin-film inductive heads for perpendicular recording," *IEEE Trans. Magn.*, vol. 26, no. 6, pp. 2966–2971, Nov. 1990.

[7] J. P. Lazzari and P. Deroux-Dauphin, "A new thin film head generation: Ic head," *IEEE Trans. Magn.*, vol. 25, no. 5, pp. 3190–3192, Sept. 1989.

[8] K. Yamasawa, K. Maruyama, I. Hirohama, and P. Biringer, "High-frequency operation of a planar-type microtransformer and its application to multilayered switching regulators," *IEEE Trans. Magn.*, vol. 26, no. 3, pp. 1204–1209, May 1990.

[9] T. Yachi, M. Mino, A. Tago, and K. Yanagisawa, "A new planar microtransformer for use in micro-switching-converters," *IEEE Trans. Magn.*, vol. 28, no. 4, pp. 1969–73, 1992.

[10] T. Yachi, M. Mino, A. Tago, and K. Yanagisawa, "A new planar microtransformer for use in micro-switching-converters," in *22nd Ann. Power Electron. Spec. Conf.*, June 1991, pp. 1003–1010.

[11] M. Mino, T. Yachi, A. Tago, K. Yanagisawa, and K. Sakakibara, "Microtransformer with monolithically integrated rectifier diodes for micro-switching converters," in *24nd Ann. Power Electron. Spec. Conf.*, June 1993, pp. 503–508.

[12] K. Yamaguchi, E. Sugawara, O. Nakajima, and H. Matsuki, "Load characteristics of a spiral coil type thin film microtransformer," *IEEE Trans. Magn*, vol. 29, no. 6, pp. 3207–3209, 1993.

[13] Dragan Maksimovic, "A mos gate drive with resonant transitions," in *22nd Ann. Power Electron. Spec. Conf.*, June 1991, pp. 527–532.

[14] S. H. Weinberg, "A novel lossless resonant mosfet driver," in *23nd Ann. Power Electron. Spec. Conf.*, June 1992, pp. 1003–1010.

[15] A. W. Kelley and J. E. Titus, "Dc current sensor for pwm converters," in *22nd Ann. Power Electron. Spec. Conf.*, June 1991, pp. 641–650.

[16] E. C. Snelling, *Soft Ferrites, Properties and Applications*, 2nd ed. Butterworths, 1988.

[17] F. N. Bradley, *Materials for Magnetic Functions.* Hayden, 1971.

[18] K. Ohashi, M. Ito, and M. Watanabe, "Application of electroplating to thin film head," *Electrochemical Society Extended Abstracts*, vol. 87, no. 2, 1987, Abstract No. 566.

[19] Simon H. Liao. "Electrodeposition of magnetic materials for thin-film heads," *IEEE Trans. Magn.*, vol. 26, no. 1, pp. 328–332, Jan. 1990.

[20] H. Dahms and I. M. Croll, "The anomalous codeposition of iron-nickel alloys," *J. Electrochem. Soc.*, vol. 112, no. 8, pp. 771–775, Aug. 1965.

[21] K. Krusch, "Sputter parameters and magnetic properities of permalloy for thin film heads," *IEEE Trans. Magn.*, vol. 22, no. 5, pp. 626–628, Sept. 1986.

[22] J. D. Freeman, "Effect of deposition conditions on the properties of thin permalloy film," *J. Appl. Phys.*, vol. 9, no. 3, pp. 421–425, May 1991.

[23] R. H. Page, C. S. Gudeman, and V. J. Novotny, "Glow discharge optical spectroscopy as a diagnostic of sputtered permalloy film composition and saturation magnetostriction," *J. Appl. Phys.*, vol. 65, no. 9, pp. 3586–3596, May 1989.

[24] R. F. Soohoo, *Magnetic Thin Films.* Harper and Row, 1965.

[25] H. H. Zappe, "Ferromagnetism for sensors and actuators," lecture notes for Mackay Lectures at Univ. of California, Berkeley, 1991.

[26] M. Prutton, *Thin Ferromagnetic Films*, Butterworths, 1964.

[27] S. Middelhoek, *Ferromagnetic Domains in Thin Ni-Fe Films*, Ph.D. dissertation, University of Amsterdam, 1961.

[28] Marvin Camras, *Magnetic Recording Handbook*, Van Nostrand Reinhold, 1988.

[29] Yuan-Zhi Shoa, Shou-Ren Gu, and Nan-Ping Chen, "Soft magnetic properties and brittleness of boron-doped sendust alloy," in *Materials Research Society Symposium Series: Magnetic Materials: Microstructure and Properties*, Apr. 1991, vol. 232, pp. 233–236.

[30] S. Wang, K. E. Obermyer, and M. H. Kryder, "Improved high moment fealn/sio$_2$ laminated materials for thin film recording heads," *IEEE Trans. Magn.*, vol. 27, no. 6, pp. 4879–4881, Nov. 1991.

[31] C. H. Ahn, Y. J. Kim, and M. G. Allen, "A fully integrated micromachined toroidal inductor with a nickel-iron magnetic core (the switched dc/dc boost converter application)," in *7th Ann. Int. Conf. Solid-State Sensors and Actuators*, 1993, pp. 70–73.

[32] D. D. Tang, "Stable encapsulation structures for permalloy films," *IEEE Trans. Magn.*, vol. 30, no. 6, pp. 5073–5078, Nov. 1994.

[33] A. C. Adams, "Dielectric and polysilicon film deposition," in *VLSI Technol.*, S. M. Sze, Ed. McGraw-Hill, 1983, ch. 3, pp. 93–129.

[34] R. S. Muller and I. Kamins, *Device Electronics for Integrated Circuits.* Wiley, 1986, p. 55.

[35] P.L. Dowell, "Effects of eddy currents in transformer windings," *Proc. IEE*, vol. 113, no. 8, pp. 1387–1394, Aug. 1966.

[36] R. W. Harcourt, O. Zorba, and A. G. Whitaker, "Competing technologies of mcms," *Electron. Eng.*, vol. 64, no. 782, pp. 57–63, Feb. 1992.

[37] V. Puri, "Effect of metalization process on the performance of passive microstripline circuits.," *Microwave Optical Technol. Lett.*, vol. 5, no. 11, pp. 585–590, Oct. 1992.

[38] M. E. Thomas, S. Sekigahama, and S. A. Myers, "Issues associated with the use of electroless copper films for submicron multilevel interconnections.," in *Proc. 7th Int. IEEE VLSI Multilevel Interconnect. Conf.*, June 1990, pp. 335–337.

[39] K. D. T. Ngo and M. H. Kuo, "Effects of air gaps on winding loss in high-frequency planar magnetics," in *19st Ann. Power Electron. Spec. Conf.*, Apr. 1988, pp. 1112–1119.

[40] Andrew Franklin Goldberg, "Development of magnetic components for 1–10 MHz dc/dc converters, Ph.D, dissertation, M.I.T., Cambridge, MA, Sept. 1988.
[41] W. M. Chew and P. D. Evans, "High frequency inductor design concepts," in *22nd Ann. Power Electron. Spec. Conf.*, June 1991, pp. 673–678.
[42] I. Sasada, T. Yamaguchi, and K. Harada, "Methods for loss reduction in planar inductors," in *23nd Ann. Power Electron. Spec. Conf.*, June 1992, pp. 1409–1415.
[43] K. Kawabe, H. Koyama, and K. Shirae, "Planar inductor," *IEEE Trans.. Magn.*, vol. 20, no. 5, pp. 1804–1806, Sept. 1984.
[44] O. Oshiro, H. Tsujimoto, and K. Shirae, "A novel miniature planar inductor," *IEEE Trans.. Magn.*, vol. 23, no. 5, pp. 3759–3761, Sept. 1987.
[45] M. Yamaguchi, S. Arakawa, S. Yabukami, K. I. Arai, F. Kumagai, and S. Kikuchi, "Estimation of the in-situ permeabilities in thin-film inductors," *IEEE Trans. Magn.*, vol. 29, no. 5, 1993.
[46] M. Yamaguchi, S. Arakawa, H. Ohzeki, Y. Hayashi, and K. I. Arai, "Characteristics and analysis fo a thin film inductor with closed magnetic circuit structure," *IEEE Trans. Magn.*, vol. 28, no. 5, 1992.
[47] U. Kirchenberger, M. Marx, and D. Schroder, "A contribution to the design optimization of resonant inductors in high power resonant converters," in *1992 IEEE Ind. Applicat. Soc. Ann. Meet.*, Oct. 1992, vol. 1, pp. 994–1001.

Charles R. Sullivan was born in Princeton, NJ, in 1964. He received the B.S. degree in electrical engineering with highest honors from Princeton University in 1987. He is working toward the Ph.D. degree in electrical engineering at the University of California, Berkeley.

Between 1987 and 1990, he worked at Lutron Electronics, Coopersburg, PA, developing high-frequency dimming ballasts for compact fluorescent lamps. He has published technical papers on numerous topics, including thin-film magnetics for high frequency power conversion, dc/dc converter topologies, energy and environmental issues, and modeling, analysis, and control of electric machines.

Seth R. Sanders (M'87) received S.B. degrees in electrical engineering and physics from the Massachusetts Institute of Technology, Cambridge, in 1981.

He worked as a design engineer at the Honeywell Test Instruments Division in Denver, CO, and returned to M.I.T. in 1983, where he received the S.M. and Ph.D. degrees in electrical engineering in 1985 and 1989, respectively. He is Assistant Professor in the Department of Electrical Engineering and Computer Sciences at the University of California, Berkeley. His research interests include power electronics, variable speed drive systems, simulation, and nonlinear circuit and system theory, as related to the power electronics field.